

Investigation of electron-irradiated zinc by diffuse x-ray scattering. I. Self-interstitials in zinc

P. Ehrhart and B. Schönfeld

Institut für Festkörperforschung der Kernforschungsanlage Jülich, D-5170 Jülich, Germany

(Received 31 July 1978)

Single crystals of zinc were irradiated at 6 K with 3-MeV electrons producing electrical resistivity changes varying from 32 to 215 nΩcm. Diffuse x-ray scattering from the irradiated samples was measured near (00.h), (h0.0), and (hh.0) reflections. From the distribution of the diffuse scattering intensity we conclude that the configuration of the self-interstitial in Zn is a dumbbell aligned along the *c* axis. A combination of lattice parameter, electrical resistivity, and Huang scattering measurements yields a volume change per interstitial of 3.6 atomic volumes (assuming a vacancy relaxation of -0.6 atomic volumes) and a specific resistivity per Frenkel pair $\rho_F = 15.3 \mu\Omega\text{cm/at. \%}$.

I. INTRODUCTION

Diffuse x-ray scattering near Bragg reflections in irradiated crystals allows the identification of the structure of radiation-induced interstitials and is particularly sensitive to the formation of defect clusters. The measurements give directly the symmetry and strength of the long-range displacement field of the defects. Previous diffuse scattering measurements on electron-irradiated metals have been restricted to cubic crystals such as Al and Cu (see Ref. 1 for a recent review). In the present work, we consider for the first time a hexagonal crystal. Zinc is of particular interest since it exhibits a well-defined recovery stage I below which we expect a statistical distribution of single interstitials and vacancies to be present following electron irradiation.² This distribution is a necessary prerequisite for the determination of the interstitial structure and of quantitative parameters such as the relaxation volume of the interstitial $\Delta V^{i,rel}$ and the specific resistivity per Frenkel pair ρ_F . In Sec. II a brief introduction to the theory of diffuse scattering is given for hcp crystals. In Sec. III we describe the experimental details. Finally in Sec. IV the results for single interstitials are discussed.

II. THEORY

A review of the theory of diffuse scattering by single interstitials and clusters has been given elsewhere.³ We consider here only those details which are necessary for the understanding of hcp crystals.

Near the Bragg reflections, the diffuse scattering by crystals containing point defects is sensitive to the long-range part of the displacement field of the defects. Assuming a linear superposition of individual displacement fields, low concentration, and a statistical distribution of defects,

we obtain for the diffuse scattering cross section S

$$S = C |F_{\mathbf{R}}|^2 |F_{\mathbf{R}}^D/F_{\mathbf{R}} - L_{\mathbf{R}}/C + i\vec{\mathbf{K}} \cdot \vec{\mathbf{t}}(\vec{\mathbf{q}})|^2, \quad (1)$$

where C is the concentration of point defects. The total defect scattering amplitude consists of the scattering amplitude of the defect itself ($F_{\mathbf{R}}^D$), the contribution from the strongly displaced atoms in the vicinity of the defect ($-L_{\mathbf{R}}/C$), and a contribution from the long-range part of the defect displacement field. $L_{\mathbf{R}}$ is the static Debye-Waller (DW) factor; $L_{\mathbf{R}}/C$ represents the effective number of atoms per defect scattering totally out of phase. $\vec{\mathbf{t}}(\vec{\mathbf{q}})$ is the Fourier transform of the displacement field around an individual defect, where $\vec{\mathbf{q}}$ is the difference between the scattering vector $\vec{\mathbf{K}}$ and the nearest reciprocal-lattice vector $\vec{\mathbf{h}}$. The interference of the scattered waves from the two atoms within the unit cell is considered by the structure factor $F_{\mathbf{R}}$ (see Ref. 4).

$\vec{\mathbf{t}}(\vec{\mathbf{q}})$ varies like q^{-1} which results from the r^{-2} dependence of the displacement field.³ Thus near the Bragg reflection ($q \ll h$, $h \approx K$) the leading term of S [Eq. (1)] will vary like q^{-2} (Huang scattering):

$$S_H = C |F_{\mathbf{R}}|^2 |\vec{\mathbf{h}} \cdot \vec{\mathbf{t}}(\vec{\mathbf{q}})|^2. \quad (2)$$

The next order term arises from the interference of the Huang scattering amplitude with the first two terms of Eq. (1) and varies like q^{-1} . That term will give us information on the static DW factor $L_{\mathbf{R}}/C$. Both terms are easily separated by looking at the symmetric and antisymmetric part of S with respect to $\vec{\mathbf{q}}$, i.e., by measuring on both sides of a reciprocal-lattice point ($\vec{\mathbf{K}} = \vec{\mathbf{h}} \pm \vec{\mathbf{q}}$):

$$\begin{aligned} S &= S_s + S_{as}, \\ S_s &= S_H + C |F_{\mathbf{R}}|^2 |F_{\mathbf{R}}^D/F_{\mathbf{R}} - L_{\mathbf{R}}/C|^2, \\ S_{as} &= -2C |F_{\mathbf{R}}|^2 |\vec{\mathbf{h}} \cdot \vec{\mathbf{t}}(\vec{\mathbf{q}})| [\text{Re}(F_{\mathbf{R}}^D/F_{\mathbf{R}}) - L_{\mathbf{R}}/C]. \end{aligned} \quad (3)$$

At small values of q , $S_s \approx S_H$. Because we are interested in the displacements far from the defect, we can consider the lattice as an elastic continuum and characterize the defects by the dipole-force tensor P_{ij} . Following Trinkaus⁵ we then obtain for an hcp crystal

$$S_H = C |F_R|^2 \left(\frac{h}{q}\right)^2 \frac{1}{V_c} \sum_{i=1}^4 \gamma^{(i)} \pi^{(i)}, \quad (4)$$

where V_c represents the volume of the unit cell.

$\pi^{(i)}$ are quadratic expressions of the dipole-force tensor P_{ij} . Using a rectangular coordinate system, with the c axis corresponding to axis 3, and axes 1 and 2 in the $[21.0]$ and $[01.0]$ directions, respectively, in the basal plane, we can write

$$\begin{aligned} \pi^{(1)} &= P_{33}^2, \\ \pi^{(2)} &= P_{23}^2 + P_{13}^2, \\ \pi^{(3)} &= 2(P_{11}^2 + P_{22}^2 + 2P_{12}^2) + (P_{11} + P_{22})^2, \\ \pi^{(4)} &= 2(P_{11}^2 + P_{22}^2 + 2P_{12}^2) - (P_{11} + P_{22})^2; \end{aligned} \quad (5)$$

$\gamma^{(i)}$ are determined from the elastic constants and the directions of \vec{q} and \vec{h} . Table I summarizes the parameter $\gamma^{(i)}$ for high-symmetry directions and reflections.

For defects with highly symmetrical displacement fields, the form of the dipole-force tensor is simplified. From symmetry considerations^{4,5} we have possible configurations of single interstitials in hcp metals: a dumbbell aligned along the c axis (H_c), an octahedral (O) or tetrahedral (T) site, or a crowdion configuration along a close-packed line (Fig. 1). In contrast to the other configurations, the dipole-force tensor of the crowdion configuration has nondiagonal elements, i.e., $\pi^{(2)} \neq 0$. Therefore, for a $(00.h)$ reflection in a $[21.0]$ direction we expect intensity only for this

configuration.

The three other configurations differ in their ratio P_{33}/P_{11} . Therefore it is useful to introduce this ratio to characterize the interstitial configuration. We compare the experimental P_{33}/P_{11} with ratios calculated from a simple Kanzaki force model in which the displacement field of the interstitial is described by central forces of the same strength on nearest-neighbor atoms only. This model yields for the c -split H_c

$$P_{33}/P_{11} = 1.5(c/a)^2(1 - 2d/c), \quad (6a)$$

and for the octahedral position O

$$P_{33}/P_{11} = \frac{3}{8}(c/a)^2, \quad (6b)$$

where a and c are the usual hcp lattice parameters. For the H_c configuration, the distance $2d$ for the dumbbell enters as a parameter. Table II shows the numerical data for an ideal hcp crystal ($c/a = \sqrt{3/3}$) and for zinc ($c/a = 1.83$). For the crowdion configuration $P_{33} = 0$, since the nearest neighbors are only two atoms in the basal plane. By considering further neighbors we still expect $P_{33}/P_{11} < 1$. The T configuration is a symmetry-determined equilibrium position only with an ideal hcp crystal. For Zn the distance of the interstitial to its neighbors at the corners of the tetrahedron (Fig. 1) are different and the exact position along the c axis may vary with the interatomic potentials used. Therefore the T position cannot uniquely be described by a simple model; nevertheless, we do not expect P_{33}/P_{11} to be much different from 1 because in equilibrium the distances to different neighbors should be comparable.

From Fig. 1 we see that the P_{ij} of the H_c , O , and T configurations have very simple forms. As a result, only two measurements of the Huang

TABLE I. Parameter $\gamma^{(i)}$ for high-symmetry directions and reflections (data for zinc). $\gamma^{(i)}$ are given in units of $10^{-26} \text{ cm}^4 \text{ dyn}^{-2}$. The low-temperature data of the elastic constants used for zinc were taken as the mean value of those from Garland (Ref. 6) and Alers (Ref. 7), given in units of $10^{11} \text{ dyn cm}^{-2}$: $c_{11} = 17.803$, $c_{33} = 6.864$, $c_{44} = 4.592$, $c_{12} = 3.62$, and $c_{13} = 5.41$.

Reflection	Direction of \vec{q}	$\gamma^{(1)}$	$\gamma^{(2)}$	$\gamma^{(3)}$	$\gamma^{(4)}$
(00.h)	[00.1]	$c_{33}^2 = 212.2$	0	0	0
	[10.0]	0	$\frac{1}{2}c_{44}^2 = 237.1$	0	0
(h0.0)	[10.0]	0	0	$\frac{1}{8}c_{11}^2 = 3.944$	0
	[00.1]	0	$\frac{1}{2}c_{44}^2 = 237.1$	0	0
(hh.0)	[11.0]	0	0	$\frac{1}{8}c_{11}^2 = 3.944$	0
	[00.1]	0	$\frac{1}{2}c_{44}^2 = 237.1$	0	0
	[11.0]	0	0	0	$\frac{1}{2}(c_{11} - c_{12})^{-2} = 0.2486$

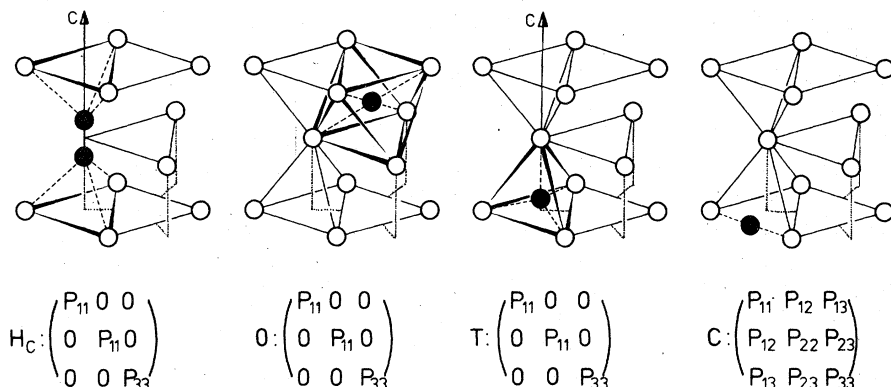


FIG. 1. Single interstitial configuration and characteristic form of the dipole-force tensor for a dumbbell (H_c), an octahedral (O), a tetrahedral (T) site, and a crowdion (C) configuration.

scattering are necessary to determine the symmetry parameter P_{33}/P_{11} : at a $(00,h)$ reflection (this yields CP_{33}^2) and at an $(h0,0)$ or $(hh,0)$ reflection (this yields CP_{11}^2). For a crowdion configuration additional measurements are necessary (see Table I).

By combination of the Huang scattering data and the lattice-parameter change⁵ which reflects the mean lattice expansion induced by the defects we can determine the concentration C and the absolute values of the components P_{ij} . Whereas the Huang scattering is proportional to CP_{ij}^2 , the lattice parameter change is proportional to CP_{ij} :

$$\frac{\Delta a}{a} = \frac{C}{\Omega} \frac{c_{33} \frac{1}{2}(P_{11} + P_{22}) - c_{13} P_{33}}{c_{33}(c_{11} + c_{12}) - 2c_{13}^2}, \quad (7)$$

$$\frac{\Delta c}{c} = \frac{C}{\Omega} \frac{c_{11} + c_{12} P_{33} - c_{13}(P_{11} + P_{22})}{c_{33}(c_{11} + c_{12}) - 2c_{13}^2}.$$

Up to this point, we have described the scattering cross section of single interstitials. If there are clusters instead of single interstitials, the above equations are valid if we consider the increase of the defect strength and the decrease of the defect concentration.

If N single interstitials form a cluster, the concentration of the single interstitials must be replaced by the concentration of the clusters, which is less by a factor of $1/N$. P_{ij}^2 of the clusters is higher by a factor of N^2 if the displacement fields of the single interstitials in a cluster superpose

TABLE II. P_{33}/P_{11} in central-force model.

	H_c	O	T	C
Ideal hcp crystal	1.6 ^a	1	1	≈0
Zn	2.3 ^a	1.3	(≈1)	≈0

^a Assuming a dumbbell distance $2d = a$.

linearly. Thus the Huang scattering per interstitial increases by a factor N :

$$S_H^c = NS_H^d. \quad (8)$$

The increase of the defect strength will restrict the Huang scattering to values of q smaller than

$$q_{cr} \approx R_0^{-1}, \quad (9)$$

where R_0 is the radius of the strongly distorted region surrounding the cluster. For $q \geq R_0^{-1}$ the scattering intensity can be described by an asymptotic approximation (Stokes-Wilson approximation), which has only been evaluated for the case of a cluster with an isotropic displacement field. The scattering cross section then reads³

$$S_{sw} = C |F_{\vec{K}}|^2 \left| \frac{\Delta V^{rel}}{4\pi\gamma} \right| \frac{h}{q^4 V_c^2} 147. \quad (10)$$

The Stokes-Wilson scattering is proportional to q^{-4} compared to the q^{-2} dependence of the Huang scattering. The numerical value 147 is correct for \vec{q} parallel to \vec{h} . Because the defect strength $\Delta V^{rel}/4\pi\gamma$ (γ is the Eshelby constant) and the concentration C enter Eq. (10) linearly, the scattering intensity in the Stokes-Wilson region is independent of the cluster size.

III. EXPERIMENT

A. X-ray measurements

The x-ray measurements were performed using an apparatus which has been described in detail elsewhere.⁸ A 6-kW rotating-anode x-ray generator with a copper target was used in combination with a quartz monochromator of the Johannson type to select $Cu K\alpha_1$ radiation. The arrangement was semifocusing with a beam divergence of 1.1° in the diffraction plane and 1.4° in the vertical plane (as defined by a Soller slit). At small distances from the Bragg reflections, resolution cor-

rections were necessary amounting to a factor of 1.9 at 1° and 1.1 at 5° from the (00.4) reflection. In order to check these corrections additional measurements with a finer resolution of 0.25° in the horizontal plane were made.

The conversion of intensities to absolute units was accomplished by comparison with the known scattering cross section of polystyrene (C_8H_8). The absorption corrections were directly determined by absorption measurements. They were small (1% - 7%) for the measurements in symmetrical Bragg geometry [(0.0*h*)-type of reflection], but varied between a factor of 1.4-1.7 for measurements in symmetrical Laue geometry [(*h*0.0)- and (*h**h*.0)-type of reflection]. The polarization factor was calculated for mosaic crystals.⁸ The structure factor $F_{\vec{h}}$ was taken from Ref. 9. Due to interference within the unit cell $F_{\vec{h},\vec{q}}$ varies with increasing q (for the maximum q corrections can be larger than 10%). In the calculation of the thermal DW factor¹⁰ we used a Debye temperature of 327 K. The lattice parameter c was measured using the Bond method and the (00.6) reflection. For the determination of the lattice parameter a no appropriate reflection with a high Bragg angle could be investigated, as it was not possible to cut a slice with an (*h*0.0) or (*h**h*.0) surface and to measure these reflections in Bragg geometry on account of the (00*h*) cleavage of zinc. Thus the low-temperature value of the unirradiated sample was calculated using the room-temperature value of $a = 2.6597 \text{ \AA}$ and the thermal expansion coefficients.¹¹⁻¹³ From these data we obtain an atomic volume $\Omega = 14.9 \text{ \AA}^3$ at low temperature.

B. Samples and irradiation

Two zinc single-crystal slices (approximately $25 \times 8 \times 0.6 \text{ mm}^3$) were spark cut from bulk material (99.999% zinc from Materials Research Corp.) and electrolytically thinned using 50 g H_3BO_3 and 100 g NaCl in 1 liter H_2O . The first slice (Zn 1) had a [01.0] rotation axis, a [00.1] surface normal and a mean thickness of 120 μm . To be able to do more precise measurements in Laue geometry, the sample was further thinned (Zn 2-4) to 25 μm thus reaching the optimal thickness $d = \mu_{\text{abs}}^{-1} = 24 \text{ \mu m}$ for zinc. The second slice (Zn 5,6) also had a [00.1] surface normal, but a [$\bar{1}$ 1.0] rotation axis and a mean thickness of 45 μm . The samples were fixed to the sample holder at only one end so they could expand freely. After mounting, the samples had mosaic spreads of typically 0.3° and residual-resistivity ratios $\rho_{RT}/\rho_{4.5 \text{ K}}$ of approximately 1000. The irradiation was performed with 3-MeV electrons in the low-temperature irradiation facility at Jülich. The samples were directly

cooled in a stream of liquid helium. The electron beam density was between 5 and 9 $\mu\text{A}/\text{cm}^2$, and the beam homogeneity over the irradiated area was better than 5%.

As a measure of the irradiation dose we used the electrical resistivity change, which was measured by a standard four-point method. The measurement was done directly on samples Zn 3 and 4. In all other cases, a separate resistivity sample of the same thickness and orientation was irradiated simultaneously with the x-ray sample. Like other hcp crystals, zinc has an anisotropic specific electrical resistivity. This was considered in determining the geometrical factor by using a room-temperature resistivity for zinc of $5.83 \text{ \mu}\Omega \text{ cm}$,¹⁴ which is appropriate for measurements in the basal plane.

After irradiation the sample was transported in a special cryostat to the measuring cryostat, keeping the sample continuously immersed in liquid helium. The resistivity was measured in liquid helium and the diffuse scattering intensity in helium gas at 6 K.

Zinc has low-temperature recovery stages: stage I_A at 5 K, I_B at 7 K (see Ref. 2). Thus after irradiation at 4.5 K and before the measurement of the diffuse scattering intensity at 6 K about 13% of the resistivity annealed (see Table III). An additional recovery of about 2% was observed during the course of the measurements. For the comparison of diffuse scattering intensity with resistivity measurements, this recovery was taken into account. In the model, which attributes stages I_A and I_B to the recombination of close Frenkel pairs, we thus expect no change in the interstitial configuration between the irradiation and x-ray measurement.

C. Discussion of measuring errors

Defects induced during the irradiation cause an increase of the diffuse scattering intensity; the defect contribution is obtained by measuring the irradiated sample and subtracting the background. This background can be measured before irradiation or after full recovery; in general there was an agreement within 5% [see Fig. 2(a)] for the symmetrical part of the background. Only at the (00.2) reflection (samples Zn 1, Zn 2) did we observe a change of the background, on the low-angle side of the Bragg reflection. There are indications that this is due to some cleavage along the (00*h*) planes during irradiation. Using only the background after full recovery for evaluation, there is good agreement with the results at other (00*h*) reflections. Nevertheless, on account of this nonreproducible background, the (00.2) re-

TABLE III. Results for Huang scattering and for lattice-parameter change.

Sample	$\Delta\rho$ (n Ω cm) ^b		η [10^3 (Ω cm) ⁻¹]	$CP_{33}^2/(\Delta c/c)$ (10^{-22} erg ²)			$CP_{11}^2/(\Delta c/c)$ (10^{-22} erg ²)		P_{33}/P_{11}
	4.5 K	6 K		(00.2)	(00.4)	(00.6)	(10.0)	(11.0)	
Zn 1 ^a	120.8	110.4		3.64	3.76		(<0.93)		(>2)
Zn 2	126.7	103.6	2.60 ± 0.39	3.60	3.79	3.55	0.75		2.21
Zn 3 ^a	31.7	27.2 ^c			3.14	3.21			
Zn 4	214.8	183.7 ^c	3.15 ± 0.27		3.33	3.46	0.66		2.27
Zn 5 ^a	211.0	127.0			(7.90)			(1.34)	(2.43)
Zn 6	153.3	134.0	3.44 ± 0.22		4.27			0.61	2.65
Average			3.05 ± 0.3		3.55 ± 0.4		0.67 ± 0.6		2.4 ± 0.3

^a Lattice-parameter change was calculated using $\eta = 3.05 \pm 0.3$ [10^3 (Ω cm)⁻¹].

^b First value of $\Delta\rho$ was measured in the irradiation cryostat, the second before the first annealing step.

^c Measured directly at the x-ray sample.

flexion was not measured in the following irradiations.

As a result of the irradiation, there will be stresses between the irradiated and unirradiated parts of the sample. This can lead to a bending of the sample, which was observed in measurements especially for Zn 4, the sample with the highest irradiation dose. Comparing its defect-scattering intensity with that of other samples, it was too low close to the Bragg reflection. Since the effect of a bending of the sample can be considered as a coarsening of the resolution, it was compensated by larger resolution corrections.

The (10.0) reflection of Zn 4 (Laue geometry) will not be so strongly affected by the bending, which is expected in a plane perpendicular to its lattice vector \vec{h} . The main error at the (10.0) and (11.0) reflections is due to the thickness variation of the sample. Therefore the measurements were done at three different spots, thus reducing the error of the absorption corrections to 6%.

For results which depend on the defect concen-

tration, the error in the lattice-parameter change measurements of 5%–15% must also be considered. The error of the Bond method has been discussed in the literature^{15–17} and is determined in our experiments by the broad mosaic spread of the crystals. For some samples, the lattice parameter was not measured directly (see Table III) but derived from the resistivity change $\Delta\rho$ using the ratio $\eta = (\Delta c/c)/\Delta\rho$ determined from other runs. If the resistivity is measured at a separate sample, additional errors may arise when the two samples contain different defect concentrations; this is not expected from the irradiation inhomogeneity (<5%), but might occur in a material with very low-temperature annealing stages by an accidental heating of one sample during the irradiation (e.g., by a short beam instability). No inconsistency of this type was observed with the results presented here.

IV. RESULTS AND DISCUSSION OF THE MEASUREMENTS AFTER IRRADIATION

A. Lattice-parameter change

After irradiation the mean lattice-parameter change was measured with Zn 2, 4, and 6 (see Table III). Within our experimental accuracy a constant ratio of $\eta = (\Delta c/c)/\Delta\rho$ is found. The results for Zn 2 and 6 agree well with Zn 4 where the electrical resistivity was measured directly on the x-ray sample. The mean value for the ratio η is 3.05×10^3 (Ω cm)⁻¹ with an estimated error of 10%.

B. Evaluation of the diffuse scattering intensity and the static Debye-Waller factor

Typical results of the diffuse scattering intensity are shown in Fig. 2. For the (00.4) reflection in a [00.1] direction [Fig. 2(a)] a strong increase after

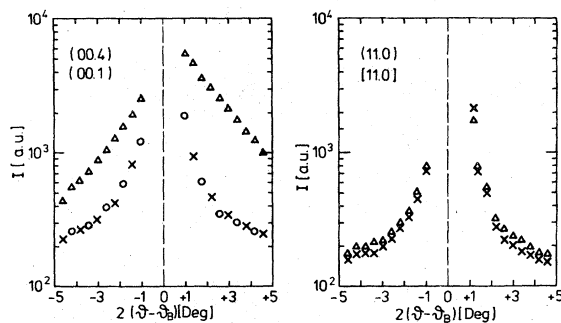


FIG. 2. Diffuse scattering intensity I before irradiation (O), after irradiation at 6 K (Δ), and after full recovery (X): (a) at h : [00.4], q : [00.1] of Zn 4; (b) at h : [11.0], q : [11.0] of Zn 6.

irradiation and strong asymmetry of the intensity are observed. On the other hand, the diffuse scattering intensity increases much less at the (11.0) reflection in a [11.0] direction and nearly no asymmetry is seen [Fig. 2(b)].

The diffuse scattering intensity can be separated into symmetrical (S_s) and antisymmetrical (S_{as}) parts with respect to \vec{q} [see Eq. (3)]. As an example Fig. 3 shows both parts at a (00.4) reflection; the symmetrical part S_H is proportional to q^{-2} , and S_{as} shows the expected q^{-1} dependence. At the (11.0) and (10.0) reflections, only S_H (proportional to q^{-2}) is shown as no q^{-1} behavior could be established due to the small asymmetry and the large statistical errors. For the symmetrical part, the constant term ($F_R^D/F_R - L_R/C$) [Eq. (3)] is normally negligible compared to Huang scattering. The high asymmetry of the defect scattering at the (00.4) reflection (S_H and S_{as} are of similar magnitude), however, indicates that this may be different for zinc.

In order to determine $F_R^D/F_R - L_R/C$, the symmetrical scattering was evaluated in a first approximation neglecting this constant term. Similar to Sec. IV C this yields the components of the dipole-force tensor $P_{11} = 11.8$ eV and $P_{33} = 29.4$ eV. With these results we can then determine $F_R^D/F_R - L_R/C$ from S_{as} . Table IV summarizes the results for the static DW factor close to the Bragg reflections. In this evaluation it has been assumed that the defect structure factor $F_R^D = f_R[2 \cos(\vec{K} \cdot \vec{d}) - 1]$ is that of the H_c configuration with a dumbbell distance $2d$ of $0.9a$. We see a very large and anisotropic static DW factor indicating that displacements along the c direction are much larger than in the basal plane. The increase of the static DW factor with the reflection order at (00. h) reflections seems reasonable although the expected $h^{3/2}$ dependence³ cannot be verified because of the large errors (the different reflection orders were not measured on the same sample).

At larger distances from the Bragg reflection the static DW factor becomes smaller, as can be seen from the deviation from the q^{-1} behavior in Fig. 3. In spite of this, its contribution to the

symmetrical scattering is only important for larger q : e.g., at $2|\vartheta - \vartheta_B| = 5^\circ$ from the (00.4) and (11.0) reflections it is 10% and at the (00.6) reflection only 2%. For all data mentioned in Sec. IV C this constant scattering contribution to the symmetrical scattering intensity has been considered. The iterative procedure was stopped after this step, since the product CP_i , which enters the static DW factor was only changed by 2%.

Measurements at (00. h) reflections in [00.1] direction were performed in three reflection orders: at the (00.2), (00.4), and (00.6) with results for the symmetrical scattering given in Figs. 4(a)–4(c). The error bars indicate the uncertainty of the resolution correction; the lower limit corresponds to corrections as given by the divergence of the x-ray beam, the upper limit considers also the mosaic width and the different bending of the samples as discussed above.

A q^{-2} dependence is observed for $q/h \leq 3 \times 10^{-2}$ at the (00.4) and up to the largest q/h of 1.4×10^{-2} at the (00.6) reflection. Table III summarizes these results. The measurements of Zn 5 were not used for a quantitative evaluation of single interstitials, because the sample was heated up to about 12 K. The 10% error of the mean value is mainly due to the lattice-parameter measurement. In addition to the verification of the q^{-2} dependence, the h^2 dependence of S_H can be tested with the results ob-

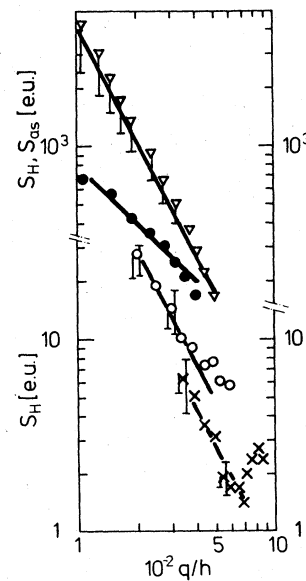


FIG. 3. Huang scattering cross section S_H at \vec{h} : (00.4), \vec{q} : [00.1] of Zn 4 (∇); at \vec{h} : (10.0), \vec{q} : [10.0] of Zn 4 (\times); at \vec{h} : (11.0), \vec{q} : [11.0] of Zn 6 (\circ); and antisymmetrical part S_{as} of the diffuse scattering intensity after irradiation at \vec{h} : (00.4), \vec{q} : [00.1] of Zn 4 (\bullet).

TABLE IV. Static Debye-Waller factor L_R/C and $\text{Re}(F_R^D/F_R)$.

Reflection	L_R/C	$\text{Re}(F_R^D/F_R)$
(00.2)	21.9 ± 10.2	≈ -1.5
(00.4)	43.0 ± 15.6	$\approx +0.5$
(00.6)	51.7 ± 22.1	≈ -1.5
(11.0)	3.9 ± 2.2	$+0.5$

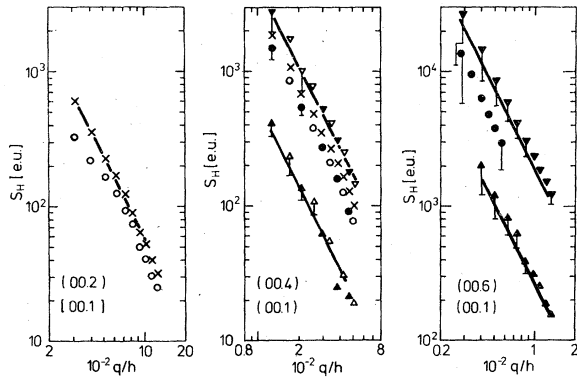


FIG. 4. Huang scattering cross section S_H after irradiation: (a) at h : (00.2), \vec{q} : [00.1] of Zn 1 (\times) and Zn 2 (\circ); (b) at h : (00.4), \vec{q} : [00.1] of Zn 1 (\times), of Zn 2 with large (\circ) and small (\bullet) incoming divergences, of Zn 3 with large (Δ) and small (\blacktriangle) incoming divergences, of Zn 4 with large (∇) and small (\blacktriangledown) incoming divergences; (c) at h : (00.6), \vec{q} : [00.1] of Zn 2 (\bullet), Zn 3 (\blacktriangle), and Zn 4 (\blacktriangledown).

tained at the three different reflection orders. We find a good agreement (within 4%) of CP_{33}^2 , measured at the (00. h) reflections for each sample.

As shown in Fig. 3 the diffuse-scattering intensity at the (10.0) reflection as measured in the [10.0] direction was considerably smaller than for (00. h) reflections. Therefore, the error in the diffuse scattering is quite large. The error bars given on the right-hand side of the points (in addition to the error due to the resolution correction) are obtained from three measurements at different sample spots. The measuring effect was increased with the second sample (Zn 5,6) on account of the higher structure factor of the (11.0) reflection. The average result for several sample spots is given in Fig. 3. The error of the average value of CP_{11}^2 is about 20%.

The q^{-2} law of the Huang scattering is fulfilled at the (10.0) and (11.0) reflections only close to the Bragg reflection for $q/h \leq 7 \times 10^{-2}$ and $q/h \leq 3.7 \times 10^2$, respectively; for larger q values the intensity decreases more slowly with q . This deviation from the q^{-2} law is consistent with the observation at the (00.4) reflection. Equation (9) yields $R_0 \approx 5.5 \text{ \AA}$; this is a reasonable value indicating that the nearest neighbors of the interstitial are strongly distorted. Table III summarizes the results at the (10.0) and (11.0) reflections. The ratio P_{33}/P_{11} is also given which is independent of the concentration C . The result of Zn 1 is neglected in the average on account of its high statistical error.

C. Symmetry and defect strength of single interstitials

As we have seen in Sec. II we can obtain information about the defect symmetry first by looking for the existence of lines of zero intensity and second from the symmetry parameter P_{33}/P_{11} .

Measurements in a [10.0] direction were done at the (00.4) reflection of Zn 1 and reproduced with Zn 2. Within the measuring range [$q/h = (3.5-7) \times 10^{-2}$] a zero line could be excluded, although compared with the [00.1] direction, the diffuse scattering intensity was much lower. These data do not show a q^{-2} dependence, but exhibit a slower decrease with q . A detailed investigation of the intensity distribution was done by making several radial scans close to the (00.4) reflection (Fig. 5). The $\omega \pm 1.5^\circ = \vartheta$ scans show zero intensity at about $2(\vartheta - \vartheta_B) = -0.5^\circ$, the $\omega + 3^\circ = \vartheta$ scan at about -2° . These results suggest a deformed zero line, as is expected at larger q values for a strongly distorting defect.¹⁸ Close to the Bragg reflection one would expect a zero line in a [21.0] direction. These measurements were prohibited by the mosaic spread of the crystals. Perpendicular to the (10.0) and (11.0) reciprocal-lattice vectors no intensity was observed. All these results suggest $\pi^{(2)} = 0$ ruling out a crowdion but not an H_c , O , or T configuration of the interstitial.

$P_{33}/P_{11} = 2.4 \pm 0.3$ (see Table III) also allows us to exclude the crowdion configuration, where we expect $P_{33}/P_{11} < 1$. The O configuration can also be excluded, since its theoretical value of 1.3 (see Table II) is much less than the experimental result. To be compatible with the experimental P_{33}/P_{11} the T configuration would yield a very unrealistic position of the interstitial along the c axis (Fig. 1) and is therefore excluded, too. Thus the single interstitial can only have an H_c configuration.

Combining Huang scattering data with the lattice-parameter change, the strength of the defect and the defect concentration can be determined. In addition to the displacement around an interstitial, the vacancy relaxation also contributes to Huang scattering and lattice-parameter change, thus yielding

$$\begin{aligned} CP_{ij}^2 &= (CP_{ij}^2)^i + (CP_{ij}^2)^v, \\ \Delta c/c &= (\Delta c/c)^i + (\Delta c/c)^v. \end{aligned} \quad (11)$$

Since $(CP_{ij}^2)^v$ and $(\Delta c/c)^v$ are not determined in our measurements, they enter the evaluation as free parameters.

From measurements of self-diffusion as a function of pressure between 300 and 400 $^\circ\text{C}$, the relaxation volume of a vacancy $(\Delta V/\Omega)^v, \text{rel} = -0.6$ has been deduced.¹⁹ This yields a dipole-force tensor

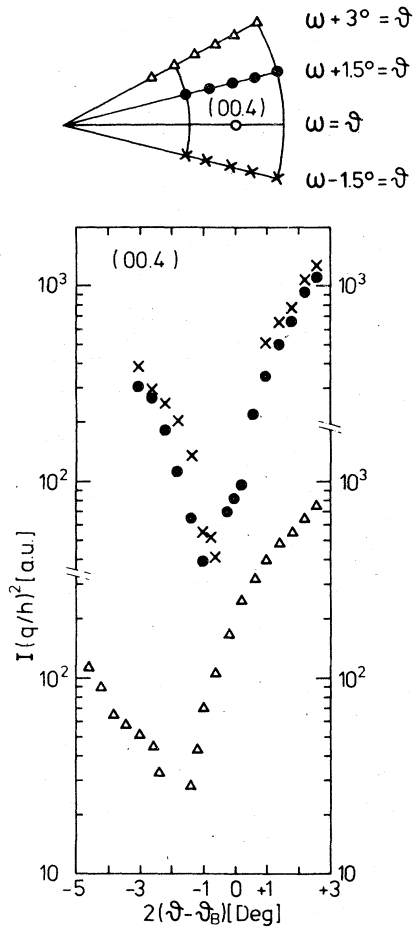


FIG. 5. Distribution of diffuse scattering intensity I after irradiation at $h: (00.4)$ of Zn 2: (a) scans in K space; (b) diffuse scattering intensity on the lines $\omega - 1.5^\circ = \theta$ (x), $\omega + 1.5^\circ = \theta$ (●), and $\omega + 3^\circ = \theta$ (Δ).

of the vacancy of $P_{ij}^v = -3.7$ eV (δ_{ij}). Although the systematic error (uncertainty in the migration volume, extrapolation to low temperatures) of this value cannot be estimated, it is expected to represent an upper limit of the vacancy contribution.

Using Eq. (7) and

$$\Delta V/V = \Delta c/c + 2\Delta a/a, \quad (12)$$

we obtain $(\Delta c/c)^v = -0.47C$ and $(\Delta a/a)^v = -0.06C$. Thus the vacancy contribution to the measured lattice-parameter change for Frenkel defects amounts to about 8% for both axes. At the $(00h)$ reflections, the vacancy contribution to the Huang scattering is negligible (about 2%), at the (10.0) and (11.0) reflections, however, it is 14%. This is due to the low value of P_{11}^i and the isotropy of the vacancy. The results both with and without consideration of the vacancy relaxation are summarized in Table V. Including this correction, P_{33}/P_{11} , for the interstitial, changes from 2.4 to 2.5. Using Eq. 6(a) the dumbbell distance was determined to be 8% less than the nearest-neighbor distance a . The specific resistivity per Frenkel defect ρ_F can be compared with the results of damage rate measurements on single crystals (for a recent review see Ref. 20). There is very good agreement with the most recent value of $(15 \pm 5)\mu\Omega \text{ cm/at.}\%$.²¹ Because ρ_F might be anisotropic in hcp crystals, it is important to emphasize that the resistivity was always measured in the basal plane. Here again the possible correction due to the influence of the vacancy is smaller than the experimental error.

The self-interstitial in Zn is characterized by a large anisotropy of its displacement field and also by a large relaxation volume of 3.6 atomic volumes. $P_{33}/P_{11} = 2.5$ corresponds to a strain-tensor ratio $\lambda_{33}/\lambda_{11} = -6.4$ (λ_{11} and λ_{33} of Ref. 1 must be scaled by a factor of 1.4). These values are in agreement with the large and anisotropic static DW factor discussed above (Table IV). The results for the self-interstitial in hcp Zn are very different from those in fcc metals like Al or Cu, where the $[100]$ -split configuration has a nearly isotropic long-range displacement field and also a much smaller relaxation volume of 1.9 and 1.45 atomic volumes, respectively, for Al and Cu. The large anisotropy may be understood from the unusual elastic behavior of Zn. Even an isotropic defect will cause a lattice-parameter change that is higher by a factor of 7 at the c axis than at the a axis (e.g., the vacancy discussed above). With an anisotropic defect such as the H_c configuration we actually observe a shrinkage in the basal plane along with the expansion of the c axis. According to Eq. (7) this occurs when $P_{33}/P_{11} < c_{33}/c_{13} (=1.3$

TABLE V. Results for self-interstitials in zinc.

$(\Delta V/V)^v$	P_{11}^i (eV)	P_{33}^i (eV)	$2d$ (a)	$(\Delta V/V)^i$	ρ_F ($\mu\Omega \text{ cm/at.}\%$)
0	11.6 ± 2.2	27.9 ± 5.1	0.95 ± 0.06	4.0 ± 0.7	18.2 ± 5.7
-0.6	10.0	25.3	0.92	3.6	15.3

for Zn). A similar decrease in the a axis along with an increase of the c axis is also observed in heating zinc single crystals from 4 to 70 K.^{11,12}

The large relaxation volume is consistent with the restricted range of the q^{-2} dependence discussed in Sec. IV B. It seems interesting to note that these changes are different at different reflection types. At (00.4) reflections we observe at large q values a more rapid decrease of the intensity than q^{-2} . This is expected for strongly distorting defects and is a first indication for the q^{-4} dependence [Eq. (10)] that is observed for even stronger defects. In contrast to this we observe a decrease of the intensity [looking at comparable q values at the (10.0) or (11.0) reflection] that is much slower than q^{-2} (Fig. 3). This may indicate that close to the defect the displacements in the basal plane are much larger than in an r^{-2} extrapolation of the long-range displacement field.

The large $(\Delta V/\Omega)^{i,rel}$ could also be explained if small clusters rather than single interstitials are formed during irradiation. Assuming $(\Delta V/\Omega)^{i,rel} \approx 1.5$ similar to Al and Cu, these clusters would contain $N=2-3$ interstitials. However, the Huang scattering cross section S_H increases with the growth of clusters [Eq. (8)]. In contrast to Au,²² and high-dose irradiated Cu,^{1,23} where a nonlinear increase of S_H with the irradiation dose or defect concentration was observed, Table III shows that for Zn the Huang scattering intensity is proportional to the defect concentration. From this we

would be forced to conclude that, beginning from the lowest irradiation dose, clusters of the same size are always formed and do not grow during the irradiation. This explanation seems to be very unlikely. Although 3-MeV electrons can initiate double or triple displacements in Zn, due to the strong dominance of small energy transfers by fast electrons the majority of the defects will be formed by single displacements. A subsequent migration process to form clusters would always lead to an increasing cluster size with dose. In addition, if there were clusters of the average size of N interstitials, the value of ρ_F would be smaller by a factor of N in contrast to other measurements.²¹ Furthermore, the annealing behavior discussed in a subsequent paper suggests the presence of single interstitials below stage I.² Therefore, we exclude the possibility of a large $(\Delta V/\Omega)^{i,rel}$ due to clustering.

ACKNOWLEDGMENTS

It is a pleasure to thank Dr. H. Trinkaus for many discussions and for making his unpublished results available to us. In addition we thank H. Koslowski, A. M. Fattah, and the staff of the Low Temperature Irradiation Facility for experimental assistance. Finally, we thank Professor W. Schilling for his continuous interest in this work, and Professor W. Schilling and Dr. J. B. Roberto for carefully reading the manuscript.

¹P. Ehrhart, *J. Nucl. Mater.* **69-70**, 200 (1978).

²H. Vandenborre, J. Nihoul, and L. Stals, *Cryst. Lattice Defects* **5**, 89 (1974).

³P. H. Dederichs, *J. Phys. F* **3**, 471 (1973).

⁴B. E. Warren, *X-Ray Diffraction* (Addison-Wesley, Reading, Mass., 1968).

⁵H. Trinkaus (unpublished).

⁶C. W. Garland and R. Dalven, *Phys. Rev.* **111**, 1232 (1958).

⁷G. A. Alers and J. R. Neighbours, *J. Phys. Chem. Solids* **7**, 58 (1958).

⁸P. Ehrhart and W. Schilling, *Phys. Rev. B* **8**, 2604 (1973).

⁹*International Tables of X-Ray Crystallography IV* (Kynoch, Birmingham, 1974).

¹⁰A. Guinier, *X-Ray Diffraction* (Freeman, San Francisco, 1963).

¹¹E. Grüneisen and E. Goens, *Z. Phys.* **29**, 141 (1924).

¹²D. A. Channing and S. Weintroub, *Can. J. Phys.* **43**, 1328 (1965).

¹³J. Donohue, *The Structure of the Elements* (Wiley,

New York, 1974).

¹⁴G. W. C. Kaye and T. H. Laby, *Tables of Physical and Chemical Constants* (Longmans, London, Green, 1973).

¹⁵W. L. Bond, *Acta Crystallogr.* **13**, 814 (1960).

¹⁶R. L. Barns, *Advances in X-Ray Analysis*, edited by K. F. J. Heinrich *et al.* (Plenum, New York, 1972), Vol. 15.

¹⁷E. E. Gruber and R. E. Black, *J. Appl. Crystallogr.* **3**, 354 (1970).

¹⁸H. Trinkaus, *Z. Angew. Phys.* **31**, 229 (1971).

¹⁹L. C. Chabildas and H. M. Gilder, *Phys. Rev. B* **5**, 2135 (1972).

²⁰P. Lucasson, in USERDA Conf. No. 751006-P1 (U. S. GPO, Washington, D. C., 1975), p. 42.

²¹P. Vajda, *Rev. Mod. Phys.* **49**, 481 (1977).

²²P. Ehrhart and E. Segura, in USERDA Conf. No. 751006-P1 (U.S. GPO, Washington, D. C., 1975), p. 295.

²³P. Ehrhart and U. Schlagheck, in USERDA Conf. No. 751006-P2 (U.S. GPO, Washington, D. C., 1975), p. 839.